

Transforming Indoor Localization: Advanced Transformer Architecture for NLOS Dominated Wireless Environments with Distributed Sensors

Saad Masrur¹, Jung-Fu (Thomas) Cheng², Atieh R. Khamesi², İsmail Güvenç¹

¹Department of Electrical and Computer Engineering, North Carolina State University, Raleigh, NC, USA

²Ericsson Research, Santa Clara, CA, USA

{smasrur, iguvenç}@ncsu.edu, {atieh.rajabi.khamesi, thomas.cheng}@ericsson.com

Abstract— Indoor localization in challenging non-line-of-sight (NLOS) environments often leads to mediocre accuracy with traditional approaches. Deep learning (DL) has been applied to tackle these challenges; however, many DL approaches overlook computational complexity, especially for floating-point operations (FLOPs), making them unsuitable for resource-limited devices. Transformer-based models have achieved remarkable success in natural language processing (NLP) and computer vision (CV) tasks, motivating their use in wireless applications. However, their use in indoor localization remains nascent, and directly applying Transformers for indoor localization can be both computationally intensive and exhibit limitations in accuracy. To address these challenges, in this work, we introduce a novel tokenization approach, referred to as Sensor Snapshot Tokenization (SST), which preserves variable-specific representations of power delay profile (PDP) and enhances attention mechanisms by effectively capturing multi-variate correlation. Complementing this, we propose a lightweight Swish-Gated Linear Unit-based Transformer (*L-SwiGLU Transformer*) model, designed to reduce computational complexity without compromising localization accuracy. Together, these contributions mitigate the computational burden and dependency on large datasets, making Transformer models more efficient and suitable for resource-constrained scenarios. The proposed tokenization method enables the Vanilla Transformer to achieve a 90th percentile positioning error of 0.388 m in a highly NLOS indoor factory, surpassing conventional tokenization methods. The *L-SwiGLU ViT* further reduces the error to 0.355 m, achieving an 8.51% improvement. Additionally, the proposed model outperforms a 14.1 times larger model with a 46.13% improvement, underscoring its computational efficiency.

Index Terms— 3GPP InF, FLOPs, indoor localization, NLOS, signal processing, tokenization, Transformer.

I. INTRODUCTION

The rapid advancement of wireless communication technologies, fueled by the deployment of 5G and the emerging vision of 6G, is driving transformative innovations in location-based services. Applications such as vehicle-to-everything (V2X) communication, urban air mobility (UAM), extended reality (XR), near-real-time robotic operations, and Smart X systems [1], [2] are at the forefront of this technological evolution. These advancements require the large-scale integration of Internet of Things (IoT) infrastructures, thereby intensifying the demand for accurate and efficient localization methods with reduced computational complexity to ensure the stringent quality of service (QoS) necessary for these cutting-edge applications. Effective indoor localization is particularly critical for applications such as navigation, safety and rescue operations, and resource optimization for customized user services. However, the need for reduced computational complexity is paramount, as most indoor positioning devices are constrained by limited computing power. Addressing these challenges requires the development of efficient and precise localization methods

capable of operating within these constraints while supporting the demands of modern wireless communication systems.

Global Navigation Satellite Systems (GNSS), commonly used for outdoor localization, face significant challenges in indoor environments due to severe channel conditions such as shadowing, fading, and noise, as well as the high probability of non-line-of-sight (NLOS) situations. Conventional wireless signal-based localization techniques [3], including Time of Arrival (TOA), Time Difference of Arrival (TDOA), Time of Flight (TOF), and Angle of Arrival (AOA), often perform poorly in highly NLOS environments, which are typical in indoor settings like factories, hospitals, shopping malls, and military installations. Additionally, these techniques frequently rely on empirical models that exhibit high complexity and a strong dependence on varying channel conditions.

Fingerprinting [4] has emerged as a widely adopted approach for indoor localization, relying on signal measurements such as Received Signal Strength Indicator (RSSI) or Channel State Information (CSI) to create location-specific fingerprints. However, traditional machine learning (ML) based fingerprinting methods often struggle to adapt to environmental variability and fail to capture the complex spatial and temporal relationships in the data. To address these limitations, researchers have increasingly turned to deep learning (DL) techniques, such as Convolutional Neural Networks (CNNs) and Multi-Layer Perceptrons (MLPs) [3], which are capable of learning more robust and discriminative features from the fingerprint data. DL-based fingerprinting techniques have shown promising results in various studies, but such techniques also increase system complexity, requiring substantial memory and processing power. This added complexity can hinder real-time implementation and scalability. Therefore, addressing these challenges is crucial, and this paper aims to present an approach that balances performance improvements with reduced system overhead, making fingerprinting techniques more efficient and adaptable.

The Transformer model [5] offers several advantages over traditional sequence processing techniques such as Recurrent Neural Networks (RNNs) and Long Short-Term Memory (LSTM) networks, including parallelization capability, reduced training time, and improved handling of long-range dependencies [6]. Transformers, despite their proven success in fields such as natural language processing (NLP), computer vision (CV), and machine translation [5], [7], have not been extensively used for indoor localization. This underutilization is largely due to the lack of inductive biases such as locality and translation invariance, which are

naturally present in CNNs but absent in Transformers, and due to the Transformer’s dependence on large datasets to capture both local and global features [7]. These challenges are further amplified by the way inputs are tokenized, which can impact the model’s training effectiveness.

In highly NLOS indoor wireless environments, multi-antenna systems face significant challenges due to multipath propagation, where signals undergo reflection, diffraction, and scattering from walls, furniture, and other obstacles. This complex propagation leads to signal superposition, causing phase shifts, fading, and interference, which further complicate the resolution of spatial and temporal variations in such environments. Moreover, in the context of indoor localization, access to large-scale datasets is limited, as collecting data of this magnitude is both computationally expensive and cost-inefficient. Additionally, existing network infrastructures lack the high computational resources necessary to test models with billions of FLOPs, which further constrains the deployment of computationally intensive models. These challenges underscore the need for more efficient approaches that reduce the dependence of Transformer-based models on large datasets while simultaneously lowering their computational complexity, enabling practical deployment in complex indoor wireless environments.

One critical yet often overlooked aspect of Transformers, particularly within the wireless communication domain, is tokenization. Conventional tokenization methods typically aggregate multiple variables, such as delayed events and physical measurements, into a single representation. This aggregation can obscure variable-specific features, leading to less informative attention maps and degrading model performance. Consequently, the model’s dependency on extensive datasets increases, as larger datasets are required to effectively map complex multi-antenna radio signals to precise locations. Therefore, in this paper, we investigate the Transformer architecture and enhance its learning capabilities by proposing a sophisticated and physically interpretable tokenization technique referred to as *Sensor Snapshot Tokenization (SST)* that leverages the characteristics of wireless communication systems, specifically addressing inherent channel independence and enabling the Transformer to effectively learn the multivariate correlations using the tokens from multi-antenna radio system. This approach facilitates the development of variate-centric representations, resulting in meaningful attention maps and leading to a decreased dependence of the Transformer on large models and extensive datasets.

To further enhance efficiency and reduce computational complexity, we introduced modifications to several components of the vanilla Transformer architecture. These include replacing conventional normalization layers, redesigning the feed-forward network, and redefining the prediction mechanism using tokens from the final encoder block. The resulting enhanced Transformer model is termed the *Lightweight Swish-Gated Linear Unit-based Transformer (L-SwiGLU Transformer)*, optimized for improved performance in resource-constrained scenarios. Furthermore, we perform a comprehensive evaluation of various architectural configurations within Transformers across datasets of varying sizes. This analysis underscores the efficacy of the proposed methodology, illuminating potential avenues for further research and development.

The primary contributions of this work are summarized as follows:

- We define indoor localization in multi-antenna systems

under highly NLOS conditions as a multivariate modeling challenge, addressed using Transformers to capture complex channel dynamics.

- We propose a novel tokenization technique, *SST*, which enables the Transformer to capture multivariate correlations and generate meaningful attention maps, significantly reducing reliance on large datasets.
- We propose *L-SwiGLU Transformer*, a modified Transformer architecture that enhances computational efficiency and positioning accuracy by replacing the MLP-based feed-forward network (FFN) with a Swish gated linear unit (GLU)-based FFN. Additionally, we replace standard components, such as the class token and normalization layers, with more efficient counterparts. Furthermore, by introducing a global average pooling layer, we demonstrate that positional embeddings can be omitted without adversely affecting positioning accuracy.
- We conduct an extensive evaluation of various Transformer architectures across datasets and models of varying sizes, demonstrating the proposed methodology’s superior accuracy and computational efficiency.

The structure of the paper is organized as follows. Section II provides a comprehensive review of the existing literature. The system model is described in detail in Section III. Section IV explains the preprocessing steps and the tokenization methods. The design of transformer architectures for processing distributed sensor signals is discussed in Section V. Extensive evaluation studies and analyses are presented in Section VI. Finally, the paper concludes in Section VII.

II. LITERATURE REVIEW

In the literature, indoor positioning is classified into two major categories: geometric-based methods and fingerprinting-based methods [3]. Geometric approaches, such as trilateration and triangulation, use parameters such as AoA, TDoA, ToF, and ToA for positioning. Although these algorithms are well-established and extensively studied, they perform poorly in indoor scenarios due to outlier distortion caused by NLOS and multipath challenges [3].

Conversely, fingerprinting methods involve creating a database by collecting signals from various locations and extracting features from them. This constructed database is then used to predict the location of new signals. Compared to geometric approaches, fingerprinting methods are relatively simple, easily integrated into smart devices, and capable of achieving acceptable accuracy with support from existing wireless infrastructure, which explains their widespread exploration in the literature [3], [8].

Most of the work involving ML-based fingerprinting has utilized shallow ML algorithms like K-nearest neighbors (KNN), Decision Trees (DTs), Support Vector Machines (SVM), and Random Forests. These algorithms are computationally expensive to train on large datasets and their performance tends to degrade. Furthermore, the performance of traditional ML methods will not scale with larger, more complex datasets [9]. With the advent of DL models, researchers have begun exploring algorithms like MLPs, RNNs, LSTMs, and CNNs for fingerprinting. Comprehensive details about deep learning-based fingerprinting methods, including the pros and cons of different methods and various types of inputs used for positioning, are provided in [3], [8].

Numerous DL techniques, including CNNs and LSTMs, have achieved remarkable success in indoor localization

[10], [11]. In [12], a fully complex-valued neural network (CVNN) was proposed for positioning in environments with moderate Line-of-Sight (LoS) conditions, demonstrating high accuracy in 2D localization tasks. Building on this work, [13] extended the approach by employing a complex-valued ResNet model tailored for highly NLoS scenarios.

With the recent success of Transformer-based models in various applications, researchers have become increasingly interested in exploring their potential for indoor localization. In [14], the Vision Transformer (ViT) [7] which in encoder only Transformer model was employed for fingerprinting-based indoor localization. The approach involved using a CNN to create patches from the CSI matrix, which were then fed into the Transformer encoder blocks for localization. Similarly, the authors in [15] used ViT for WiFi-assisted indoor localization. They applied Principal Component Analysis (PCA) for input normalization and created RSSI gray images from the normalized RSSI data, achieving a 50th percentile error of 1.788 m. However, the use of PCA makes this approach impractical for real-world applications, as the same transformation cannot be consistently applied during testing, leading to performance degradation. Additionally, the dataset used in this study is not publicly available, making it difficult to assess the proportion of LOS.

In [9], a Transformer encoder-only network is utilized for Received Signal Strength (RSS) based WiFi fingerprinting, where the values from wireless access points (WAPs) serve as inputs. The study focuses on building floor and room prediction tasks using RSS data. However, since only a single RSS value per WAP is available, the model's ability to extract meaningful spatial or temporal features is inherently limited. Furthermore, the use of PCA as a pre-processing step may not be optimal.

The authors in [16] proposed a hybrid model incorporating CNNs and ViT for localization in Long Range Wide Area Network (LoRaWAN). In this model, CNN is used to learn local features while ViT captures global features. Similarly, in [17], the authors presented a CNN-aided ViT-based indoor localization method. In this approach, the CSI matrix is treated as an image and fed into a CNN, with the resulting features used as patches for the ViT. In the context of indoor localization for MIMO systems, the study in [18] adopts a similar hybrid approach, utilizing a variant of the ViT alongside a CNN for feature extraction.

An approach described in [19] employs a Transformer for signal source localization using the AoA, creating images based on the reference point's location and arrival angle. However, the process for generating these images is not explained. Additionally, this method utilizes both the encoder and decoder parts of the Transformer, which is unusual since typically only the encoder is used for classification and regression tasks. The work and rationale for this architectural choice are also not provided. ViT have also been investigated for human activity recognition (HAR) using WiFi CSI [20]. In this approach, the raw CSI data is transformed into a CSI spectrogram, which is then used as input to the ViT model for effective HAR.

In the studies discussed, the input data was predominantly treated as images, with ViTs employed as localization algorithms without any modifications to their architecture. Although this approach capitalizes on ViT's inherent strengths in processing image data, it fails to fully exploit the unique characteristics of wireless communication systems. Specifically, wireless environments exhibit phenomena such as channel independence, signal fading, and multipath prop-

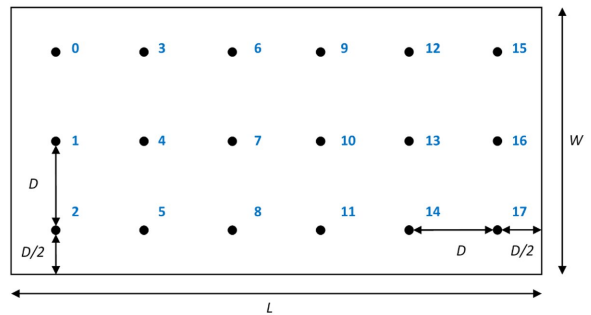


Fig. 1: 3GPP Indoor Factory (InF) layout with $N_S = 18$ sensor nodes. For the InF-DH scenario, the dimensions are $L = 120$ m, $W = 60$ m and $D = 20$ m, with 60% of the area covered by clutters of 6m height and 2m size.

agation, which are critical for accurate localization. By treating the data solely as visual inputs, these approaches overlook the rich temporal and spatial correlations that are fundamental to wireless communication. Ineffective utilization of the transformer architecture results in an increased reliance on larger Transformer models and necessitates the use of extensive datasets. Furthermore, in all these studies, the computational aspects of the resource-intensive Transformer models are largely overlooked, highlighting a significant challenge for their implementation in real-time, resource-constrained environments.

III. SYSTEM MODEL

We consider an indoor factory scenario with dense clutter and High sensor height (InF-DH) as in Fig. 1, which illustrates the spatial layout of the 3GPP InF-DH environment, including the arrangement of the sensor nodes connected to a 5G base station, operating at 3.5 GHz with a signal bandwidth of 100 MHz. A total of $N_S = 18$ sensor nodes are uniformly distributed, spaced 20 m apart, with the perimeter sensor nodes located 10 m from the walls. The heights of the sensor nodes and devices are fixed at 8 m and 1.5 m, respectively. The spatial coordinates of the r -th sensor are represented as $\psi_r = [x_s^r, y_s^r, z_s^r]^T \in \mathbb{R}^3$. The positions of all N_S sensors are then collectively represented by $\mathbf{P} = [\psi_1 \psi_2 \dots \psi_{N_S}] \in \mathbb{R}^{3 \times N_S}$, where each column corresponds to the coordinates of a single sensor. A single transmit antenna port is assumed for the device. Each sensor node is equipped with a dual-polarized receive antenna, enabling the reception of multi-antenna signals (MAS) through $A=2$ antenna ports. The RF channels between a device and the sensor nodes are generated using the 3GPP channel model documented in 3GPP Technical Report 38.901 [21].

The 3GPP InF-DH environment features a variety of obstructions, such as small to medium-sized metallic equipment and irregularly shaped items like assembly and assorted machinery. In this paper, we focus on the InF-DH {60%, 6 m, 2 m} configuration where 60% of the environment is covered by clutters of 6m height and 2m width/length. The LoS probability between a device and a sensor node is 0.008, based on empirical observations from the dataset for the InF-DH scenario [21]. That is, a LoS link between a device and the distributed sensor nodes is very unlikely. To locate a device, the device is configured to transmit the 5G sounding reference symbols (SRS) $\{s_k\}_{k=-N/2}^{N/2-1}$, where $N = 3264$ is the number of SRS subcarriers, in the uplink to be received by the 18 sensor nodes. The device transmit power is assumed 23 dBm. The SRS signals have a comb spacing of $K_{TC} = 2$

subcarriers with $\Delta_f = 30$ kHz subcarrier spacing and offset between $N_{\text{symp}} = 2$ consecutive OFDM symbols. The signal being sampled by each sensor node at a rate of $f_s = 4096 \cdot \Delta_f = 122.88$ MHz is converted into the frequency domain (FD) using an FFT of size $N_{\text{FFT}} = 4096$. Assuming L channel taps with complex gains $\{c_{a,l}\}_l$ and delays $\{\tau_l\}_l$, the received SRS at the $(k + \frac{N}{2})$ -th sub-carrier at receive antenna port a is given by

$$R_a[k] = s_k \sum_{l=0}^{L-1} c_{a,l} \exp(-j2\pi k \Delta_f \tau_l) + W_a[k], \quad (1)$$

where $W_a[k]$ is the received noise. The bandwidth of the SRS signal is $N \cdot \Delta_f = 97.92$ MHz. The measured FD channel response (CR) is obtained as

$$H_a[k] \triangleq s_k^* R_a[k]. \quad (2)$$

Assuming low mobility, the combed but offset FD CRs from the two consecutive OFDM symbols are coalesced into a combined FD CR for all subcarriers. The measured time domain (TD) channel impulse response (CIR) is obtained by further applying an inverse FFT:

$$\{h_a[d]\}_d \triangleq \text{IFFT}_{N_{\text{FFT}}} \left(\{H_a[k]\}_{k=-\frac{N}{2}}^{\frac{N}{2}-1} \right). \quad (3)$$

where d represents the discrete delay index. The TD power delay profile (PDP) is obtained by summing the powers over the antenna ports for each sample:

$$p[d] \triangleq \sum_{a=0}^{A-1} |h_a[d]|^2. \quad (4)$$

The PDP can be truncated to the first $N_{\text{ts}} = 128$ time samples without losing much information about the link between a device and a sensor node. Note that we intentionally keep the processing of the received RF signals to the minimum and leave any signal processing (e.g., filtering, smoothing, or channel estimation) to the DL model.

With $N_S = 18$ sensor nodes, each device position can be considered to map uniquely to a PDP matrix Ψ of dimensions $N_S \times N_{\text{ts}}$, with each row capturing the PDP at a different sensor. We considered three datasets, namely small, medium, and large, sampling 10,000, 20,000, and 40,000 uniformly randomly placed device locations, respectively, and recorded the corresponding PDPs. For the test datasets, we sample another 4,000 uniformly randomly placed device locations and the corresponding TD PDPs. The PDPs collected from the $N_S = 18$ sensor nodes are used as inputs to the DL model (to be defined in Section V) for joint processing, which will then output the 2D coordinates of the device.

IV. PROPOSED FRAMEWORK FOR PREPROCESSING AND TOKENIZATION

In this section, we present the proposed preprocessing technique designed for efficiently handling distributed MIMO sensor signals. Following this, we detail the conventional tokenization methods employed as benchmarks and introduce the proposed tokenization technique, which represents a significant advancement in the processing pipeline. This novel method is specifically tailored to address the limitations of existing approaches, thereby enhancing the representation and utilization of the sensor signal data.

A. Pre-processing for RF Signals from Distributed Sensors

One major issue with processing distributed sensor network signals in a DL model is the wide dynamic range

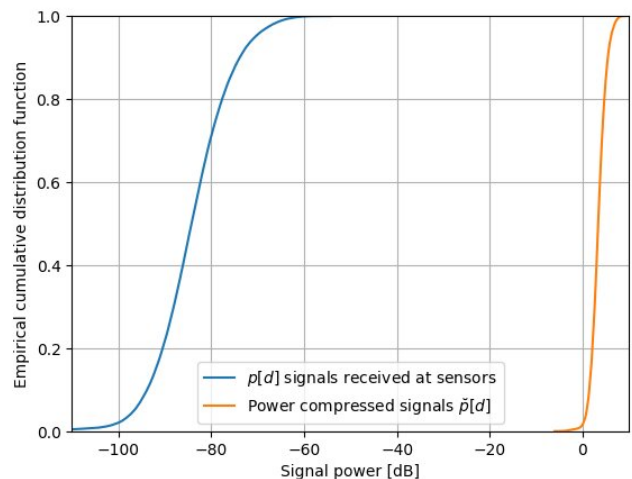


Fig. 2: Cumulative distribution function (CDF) of the received signal powers at different sensor nodes before and after power compression.

of the received signals. Because of path losses, reflection, shadowing, and fast fading effects, the received signal powers at different sensors can differ by over 35 dB as illustrated by the cumulative distribution function (CDF) in Fig. 2. Without proper handling, a DL model will ignore weaker received signal streams.

To address this dynamic range issue, we apply the power compression algorithm [13] on the PDP before feeding the signals to the DL model. For a length- N_{ts} PDP $p[d]$, the power-compressed signal is given by:

$$\check{p}[d] = S^2 \|\{p[d]\}\|^{\frac{1}{r}-1} p[d], \quad (5)$$

where $\|\{p[d]\}\| = \sum_{d=0}^{N_{\text{ts}}-1} p[d]$ is the total received power at a sensor over all its antenna ports, r is the amplitude compression ratio parameter and S is the target scale parameter after compression. For our indoor factory scenario in Fig. 1, we use $r = 5$ and $S = 10$ to compress the received signal powers into a narrower range between 0 and 10 dB illustrated in Fig. 2. Furthermore, we found better performance is obtained when using square root PDP, $\sqrt{\check{p}[d]}$, instead of straight PDP.

B. Conventional Tokenization Approaches

Patch-based Tokenization (PBT): In the wireless positioning literature, Transformer inputs are often represented in image format, with some approaches treating the CSI matrix as an image [17], and others converting RSSI and AoA data into images [15], [19]. For the first tokenization approach, similar to methods used in wireless literature, the PDP Ψ which is a matrix of dimensions $N_S \times N_{\text{ts}}$, is treated as a 2D image. This image is partitioned into fixed-size patches (referred to as tokens) with dimensions $W_h \times W_w$, where W_h and W_w denote the height and width of each token, respectively. Consequently, the total number of tokens generated from the PDP is given by $N_{\text{tk}} = \frac{N_S}{W_h} \cdot \frac{N_{\text{ts}}}{W_w}$. Each token is then reshaped into a flattened vector, resulting in a spatial size (i.e., number of sample per token) of $N_{\text{st}} = W_h \cdot W_w$, this tokenization technique is referred to as *Patch-based Tokenization (PBT)*. However, transforming inputs into image format and applying patching techniques fuses information from distinct physical measurements without considering the physical meaning of samples, which may hinder the Transformer from learning meaningful attention

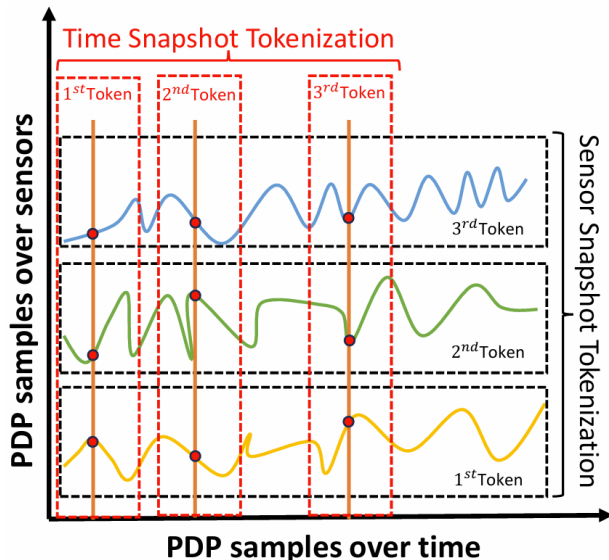


Fig. 3: Example of PDP tokenization techniques for $N_S = 3$ sensors. The proposed *Sensor Snapshot Tokenization (SST)* treats each sensor's PDP vector of size $1 \times N_{ts}$ as a token, while the alternative *Time Snapshot Tokenization (TST)* uses vectors of time samples across all sensors at a single time instant as tokens.

maps without effectively capturing the nuances of wireless communication environments. The PBT framework has not been previously utilized in conjunction with PDP in the literature. To the best of our knowledge, this paper is the first to explore its application with PDP.

C. Proposed Tokenization Approaches

In this section, we introduce two novel tokenization approaches¹—*Time Snapshot Tokenization (TST)* and *Sensor Snapshot Tokenization (SST)*. While both methods are designed to enhance feature representation in wireless communication systems, SST is the primary focus of this work due to its superior ability to capture spatial features and address the limitations of traditional input formulations. TST is presented as a complementary approach to highlight the strengths of SST.

Time Snapshot Tokenization (TST): We have $N_S = 18$ sensors; for illustration, assume that the representation of the PDP from 3 sensors is depicted in Fig. 3. The second tokenization technique, referred to as *Time Snapshot Tokenization (TST)*, represents the PDP values from all N_S sensors at a single time step as a single token, resulting in $N_{tk} = N_{ts}$ tokens, each with a dimensionality of $N_{st} = N_S$, effectively embedding multivariate temporal information within each token. When these temporal tokens are input into the multi-head attention (MHA) (to be defined in Section V) mechanism, the model tends to prioritize numerical values over the semantic relationships inherent among samples taken at the same time. Furthermore, since the values in each token are derived from different sensors, they may embody entirely distinct meanings, leading to the loss of multivariate correlations.

Tokens generated from this tokenization technique suffer from excessively localized receptive fields and will not be able to convey meaningful information, as each token is

¹Both SST and TST can be considered as special cases of *PBT*; however, these specific approaches have not been studied in the literature.

based on a single time sample across N_S sensors. Given that variations in time series data are heavily influenced by the order of the sequence, the permutation-invariant nature of the MHA mechanism is ill-suited for such data structures. As a result, the Transformer's ability to capture essential time series representations and portray multivariate correlations is diminished, thereby limiting its capacity and generalization ability across diverse time series datasets.

Sensor Snapshot Tokenization (SST): Considering the limitations of the previously discussed tokenizations we reflect on the Transformer's poor performance and propose an efficient way for tokenization technique called *Sensor Snapshot Tokenization (SST)*. This approach independently embeds each PDP series received by a sensor into a distinct token, as illustrated by the black dashed boxes in Fig. 3. Where the number of tokens is given by $N_{tk} = N_S$, with each token having a dimensionality of $N_{st} = N_{ts}$. This independent embedding enhances the receptive field, enabling the Transformer model to learn meaningful representations. Importantly, this tokenization strategy acknowledges that the information from each sensor operates independently, reflecting channel independence between sensors. Each token encapsulates a unique physical meaning, allowing Transformer to focus more on the semantic relationships among time samples rather than their numerical values.

The resulting tokens represent the global characteristics of the series, producing variate-centric tokens, and this approach allows the MHA to cross-query and correlate received signals from all sensor nodes in parallel to capture multi-variate correlations. This is aligned with the conventional signal processing principle of processing signals from all sensors/antennas jointly. Capturing multi-variate correlation relationships enhances the interpretability of our models, especially since the spatial arrangement of the sensors remains consistent throughout, these correlations reflect the relative positions and interactions between sensors, which can provide valuable clues about the location of the signal source. These factors will decrease the heavy dependence of Transformer on large datasets. Additionally, an MLP will effectively derive generalizable representations from these tokens.

The second critical aspect of the *SST* technique is its potential to achieve reduced computational complexity. The MHA layer, the most computationally heavy block of a Transformer, exhibits quadratic complexity with respect to the number of tokens. In the first approach, *PBT*, the number of tokens depends on the parameters W_h and W_w ; smaller parameter values result in a higher number of tokens. Larger values lead to less number of tokens but will aggregate information across multiple physical measurements. This aggregation can dilute variable-specific representations and lead to less informative attention maps. In contrast, the second approach *TST* maintains a token count of $N_{tk} = N_{ts}$, while the third approach *SST* has $N_{tk} = N_S$. Given that $N_S \ll N_{ts}$, the complexity of the third approach is significantly lower, resulting in greater computational efficiency.

V. DESIGNING TRANSFORMER MODEL FOR DISTRIBUTED SENSOR NETWORKS

With the recent success of encoder-only Transformer architectures like ViT in computer vision, there has been growing interest in adapting them for indoor positioning. However, directly applying ViT to this domain results in suboptimal performance and significantly increases model complexity. In this paper, we propose leveraging an encoder-

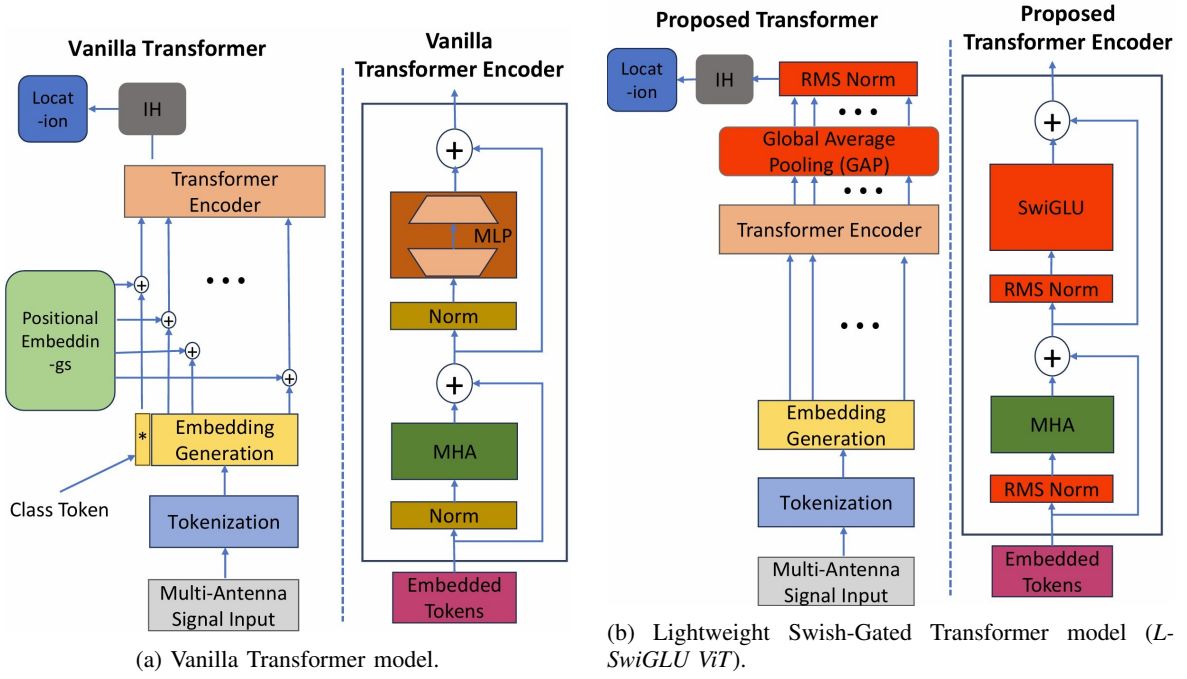


Fig. 4: The architecture of the vanilla Transformer model (Fig. 4a), while the proposed lightweight Swish-Gated Transformer (Fig. 4b), with the modified parts highlighted in red.

only Transformer model for device localization in cluttered indoor environments characterized by highly NLOS conditions. Specifically, the Transformer is designed to learn the complex mapping f between the device's position $\hat{\mathbf{y}} = [x_d, y_d]$ and the PDP Ψ received from all sensor nodes N_S , as expressed by:

$$\hat{\mathbf{y}} = f(\mathbf{P}, \Psi; \Theta), \quad (6)$$

where Θ encapsulates the model parameters, and \mathbf{P} is the sensor position vector as defined in Section III. The PDP, obtained from channel measurements at the sensors, encodes the multipath propagation characteristics by capturing the power and delay of reflected and scattered signals. This information inherently represents the spatial geometry and structure of the environment, enabling the Transformer to accurately learn the relationship between the PDP and the device's position $\hat{\mathbf{y}}$.

In this section, we describe the architecture of the vanilla Transformer model (i.e., ViT) and the proposed lightweight Swish-Gated Linear Unit-based Transformer model, referred to as L -SwiGLU Transformer. The complete architecture of vanilla Transformer and L -SwiGLU Transformer model can be seen in the Fig. 4.

A. Vanilla Transformer Architecture

Fig. 4a illustrates the architecture of the vanilla Transformer model. The localization process using a Transformer can be categorized into 3 main steps: 1) Input Embedding Preparation 2) Encoder Mechanism, and 3) Position Estimation.

1) **Input Embedding Preparation:** In the embedding preparation, the PDP input is first converted into tokens/patches $\mathbf{X}_{\text{PDP}} \in \mathbb{R}^{N_{\text{tk}} \times N_{\text{st}}}$ using the tokenization method, where N_{tk} is the number of tokens generated from PDP input, and N_{st} is the number of samples in each token. After this, the PDP tokens \mathbf{X}_{PDP} are linearly projected to create embeddings from the input using a learnable projection, $\mathbf{E} \in \mathbb{R}^{N_{\text{st}} \times D_{\text{emb}}}$ resulting in $\mathbf{X}_{\text{inp}} = \mathbf{X}_{\text{PDP}}\mathbf{E} \in \mathbb{R}^{N_{\text{tk}} \times D_{\text{emb}}}$ where D_{emb} is the dimensionality of

the embeddings. Embeddings are a way to represent data in a continuous vector space, where each PDP token is mapped to a dense, one-dimensional representation. This process captures the essential features of the PDP tokens, making it easier for the model to learn patterns and make predictions.

The next step involves appending a learnable embedding, referred to as the class token $\mathbf{X}_{\text{cls}} \in \mathbb{R}^{1 \times D_{\text{emb}}}$, to the sequence of embeddings generated from the input \mathbf{X}_{inp} . This class token serves as a global representation for the model. A classification head will be attached to it for making predictions. The resulting embedding sequence is represented as $\mathbf{X}_{\text{emb}} = [\mathbf{X}_{\text{inp}}, \mathbf{X}_{\text{cls}}] \in \mathbb{R}^{\tilde{N}_{\text{tk}} \times D_{\text{emb}}}$. The total number of tokens in embedding \mathbf{X}_{emb} will be $\tilde{N}_{\text{tk}} = N_{\text{tk}} + 1$, where 1 comes from the additional class token \mathbf{X}_{cls} . Embeddings are further encoded by positional embeddings resulting in:

$$\tilde{\mathbf{Z}} = \mathbf{X}_{\text{emb}} + \mathbf{E}_{\text{pos}}, \quad (7)$$

where $\mathbf{E}_{\text{pos}} \in \mathbb{R}^{\tilde{N}_{\text{tk}} \times D_{\text{emb}}}$ are learnable parameters that capture positional information.

2) **Encoder Mechanism:** The encoded PDP tokens $\tilde{\mathbf{Z}}$ are subsequently processed by the N_L Transformer encoder blocks, with each encoder block comprised of four primary components: the Multi-Head Attention (MHA) block, the MLP, residual connections, and a normalization layer. The main component that distinguishes the transformer from other DL models is the MHA mechanism. In this mechanism, the embeddings interact to exchange and share information. Within the attention block, communication is facilitated by projecting the encoded embedding matrix $\tilde{\mathbf{Z}}$ to generate the Queries (\mathbf{Q}), Keys (\mathbf{K}), and Values (\mathbf{V}) matrices. This is achieved using learnable weight matrices $\mathbf{W}_q \in \mathbb{R}^{D_{\text{emb}} \times d_q}$, $\mathbf{W}_k \in \mathbb{R}^{D_{\text{emb}} \times d_k}$, and $\mathbf{W}_v \in \mathbb{R}^{D_{\text{emb}} \times d_v}$, respectively, as follows:

$$\begin{aligned} \mathbf{Q} &= \tilde{\mathbf{Z}}\mathbf{W}_q, & \mathbf{K} &= \tilde{\mathbf{Z}}\mathbf{W}_k, & \mathbf{V} &= \tilde{\mathbf{Z}}\mathbf{W}_v, \\ \mathbf{Q} &\in \mathbb{R}^{\tilde{N}_{\text{tk}} \times d_q}, & \mathbf{K} &\in \mathbb{R}^{\tilde{N}_{\text{tk}} \times d_k}, & \mathbf{V} &\in \mathbb{R}^{\tilde{N}_{\text{tk}} \times d_v}. \end{aligned} \quad (8)$$

The attention mechanism (Fig. 5) is applied to (\mathbf{Q}), (\mathbf{K}),

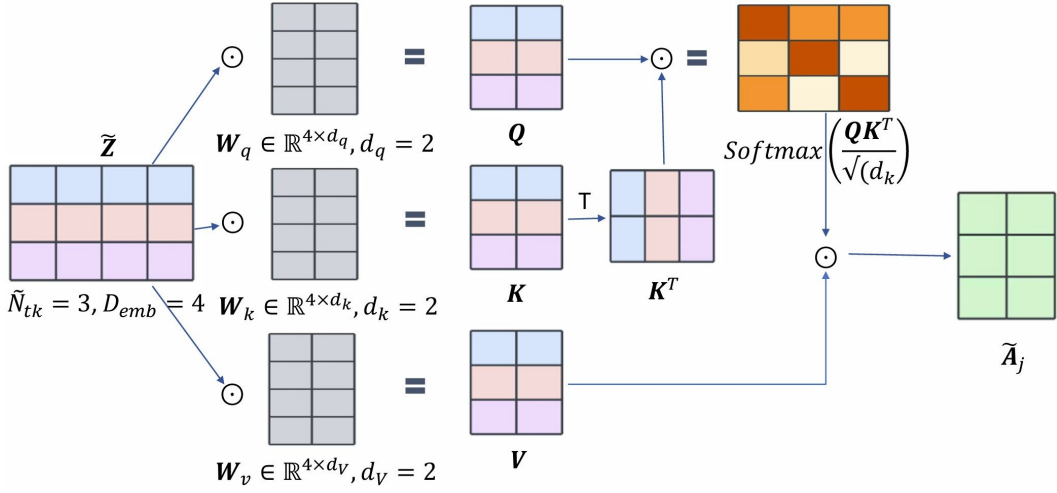


Fig. 5: Scaled dot-product attention mechanism with $\tilde{N}_{tk} = 3$ tokens and embedding dimension $D_{emb} = 4$. The input $\tilde{\mathbf{Z}}$ is projected into \mathbf{Q} , \mathbf{K} , and \mathbf{V} using weight matrices \mathbf{W}_q , \mathbf{W}_k , and \mathbf{W}_v , and attention is computed using the scaled dot product of \mathbf{Q} and \mathbf{K}^T .

and (\mathbf{V}) matrices to compute the correlation matrix $\mathbf{C} \in \mathbb{R}^{\tilde{N}_{tk} \times \tilde{N}_{tk}}$, defined as:

$$\mathbf{C} = \left(\frac{\mathbf{Q}\mathbf{K}^T}{\sqrt{d_k}} \right), \quad (9)$$

where $d_k = D_{emb}$ serves as the normalization term. The resulting correlation matrix \mathbf{C} quantifies the similarity between tokens, with each element representing the degree of correlation between corresponding token pairs. Then, the softmax is applied along the rows to turn similarity values into probabilities.

The attention score \mathbf{A}_j in the j^{th} Transformer encoder block, where $j \in \{1, 2, \dots, N_L\}$ and N_L is the total number of Transformer encoder blocks, is computed as:

$$\tilde{\mathbf{A}}_j(\mathbf{Q}, \mathbf{K}, \mathbf{V}) = \text{Softmax}(\mathbf{C})\mathbf{V} = \text{Softmax}\left(\frac{\mathbf{Q}\mathbf{K}^T}{\sqrt{d_k}}\right)\mathbf{V}, \quad (10)$$

where $j \in \{1, 2, \dots, N_L\}$. This operation assigns a weighted sum of the values (\mathbf{V}) to each embedding, where the weights are determined by the similarity between the query (\mathbf{Q}) and key (\mathbf{K}) vectors. The similarity calculation is essential, as it enables the model to learn relationships between tokens by distributing attention based on relevance, rather than solely relying on exact matches between \mathbf{Q} and \mathbf{K} .

In [7], the authors hypothesized that instead of projecting the embeddings to generate \mathbf{Q} , \mathbf{K} and \mathbf{V} one time, it is more beneficial to project it N_h times using N_h different learnable weight matrices \mathbf{W}_q^i , \mathbf{W}_k^i , and \mathbf{W}_v^i , $i \in (1, \dots, N_h)$, where N_h denotes the total number of heads. In this way, the model can learn N_h different representations from the input embeddings. To maintain the computational complexity of the multi-head attention, block similar to that of the single-head block, one can choose $d_q^i = d_k/N_h$, with the same selection for d_k^i and d_v^i . The overall complexity of MHA attention layer is $O(\tilde{N}_{tk}^2 D_{emb})$.

After the attention for all heads is calculated, the output is concatenated into a single matrix with the help of the projection weight matrix $\mathbf{W}_o \in \mathbb{R}^{N_h d_o \times D_{emb}}$, as follows:

$$\mathcal{H}_j^i = \tilde{\mathbf{A}}_j \left(\mathbf{Q} = \tilde{\mathbf{Z}}\mathbf{W}_q^i, \mathbf{K} = \tilde{\mathbf{Z}}\mathbf{W}_k^i, \mathbf{V} = \tilde{\mathbf{Z}}\mathbf{W}_v^i \right),$$

$$\text{MHA}(\tilde{\mathbf{Z}}) = \text{Concat} \left(\mathcal{H}_j^1, \dots, \mathcal{H}_j^{N_h} \right) \mathbf{W}_o.$$

Before entering every block, the input is normalized using a LayerNorm (LN), and the output is then added to the input through a residual connection to help with gradient flow and optimization:

$$\tilde{\mathbf{Z}}_j^{\text{MHA}} = \text{MHA} \left(\text{LN} \left(\tilde{\mathbf{Z}}_{j-1} \right) \right) + \tilde{\mathbf{Z}}_{j-1}. \quad (11)$$

The LN operation for the input vector $\tilde{\mathbf{Z}}_{l-1}$ is defined as:

$$\text{LN}(\tilde{\mathbf{Z}}_{j-1}) = \gamma \odot \left(\frac{\tilde{\mathbf{Z}}_{j-1} - \mu}{\sqrt{\sigma_{\text{LN}}^2 + \epsilon}} \right) + \beta,$$

where μ and σ_{LN}^2 represent the mean and variance of $\tilde{\mathbf{Z}}_{l-1}$, respectively, and γ and β are learnable parameters.

The next key component of a Transformer is the MLP block, which comprises two layers. This block is responsible for learning the information encoded in each embedding. The first layer maps the input to a higher dimension called hidden dimension h_{dim} , and the second and last layer maps it to the D_{emb} again. Therefore, the input and output of the transformer block will have a similar shape.

$$(\tilde{\mathbf{Z}}_j^{\text{MHA}}) = \mathbf{W}_j^2 \left(\sigma \left(\mathbf{W}_j^1 \tilde{\mathbf{Z}}_j^{\text{MHA}} + b_j^1 \right) \right) + b_j^2, \quad (12)$$

where σ is the activation function and \mathbf{W}_j^1 , \mathbf{W}_j^2 , b_j^1 , and b_j^2 are the weight and biases of MLP layers in j^{th} Transformer block.

Similar to the MHA block, for output of j^{th} encoder block an LN is applied before the MLP block, followed by a residual connection:

$$\tilde{\mathbf{Z}}_j^{\text{ENC}} = \text{MLP}_j \left(\text{LN} \left(\tilde{\mathbf{Z}}_j^{\text{MHA}} \right) \right) + \tilde{\mathbf{Z}}_j^{\text{MHA}}. \quad (13)$$

3) **Position Estimation:** The first embedding, referred to as the class token $(\mathbf{X}_{\text{cls}})$, is designed to capture a global representation by interacting with all other tokens through the attention mechanism. After processing through the N_L^{th} Transformer encoder block, the class token $(\mathbf{X}_{\text{cls}})$ is forwarded to an inference head (IH) which consist of one fully connected layer to generate the final predictions $\hat{\mathbf{y}}$:

$$\hat{\mathbf{y}} = \text{IH}(\tilde{\mathbf{Z}}_{N_L}^{\text{ENC}}(0)). \quad (14)$$

B. Proposed L-SwiGLU ViT

This subsection provides a comprehensive step-by-step explanation of the modifications made to the Transformer

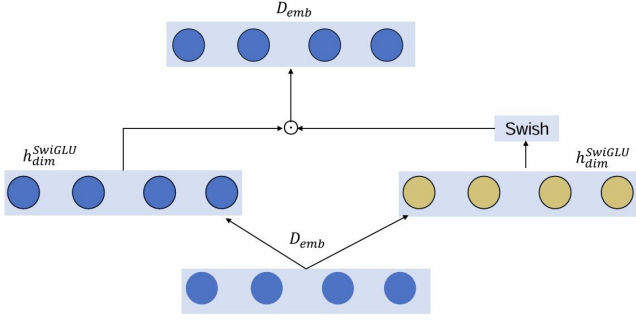


Fig. 6: GLU mechanism: one linear projection is gated via Swish activation, while the other bypasses activation; their element-wise product (\odot) filters relevant features.

components. The Fig. 4b depicts the architecture of the proposed *L-SwiGLU Transformer* model, highlighting the introduced enhancements. The modifications made in the proposed model are categorized into two parts: 1) Modifications Within the Transformer Encoder Block, and 2) Modifications Outside the Transformer Encoder Block. These modifications are detailed in the following subsections.

1) **Modifications Within the Transformer Encoder Block:** To enhance the stability, robustness, and overall performance of the *L-SwiGLU* model, the standard LN used in the vanilla Transformer model is replaced with a Root Mean Square (RMS) normalization layer. LayerNorm performs both re-centering and re-scaling, making it robust to shift noise in inputs and weights. However, in line with the hypothesis proposed in [22]—which suggests that the success of LN is attributed primarily to its re-scaling invariance rather than re-centering invariance—we substitute LN with RMSNorm. RMSNorm exclusively preserves re-scaling invariance while omitting re-centering, aligning with this hypothesis to further optimize the model’s performance. The RMSNorm operation for the input $\tilde{\mathbf{Z}}_{j-1}$ is defined as:

$$\text{RMSNorm}(\tilde{\mathbf{Z}}_{j-1}) = \frac{\tilde{\mathbf{Z}}_{j-1}}{\text{RMS}(\tilde{\mathbf{Z}}_{j-1})} \odot \gamma, \quad (15)$$

$$\text{where } \text{RMS}(\tilde{\mathbf{Z}}_{j-1}) = \sqrt{\frac{1}{n} \sum_{m=1}^n (\tilde{\mathbf{Z}}_{j-1}^{(m)})^2}.$$

Here, γ is a learnable scaling parameter, and RMSNorm avoids the mean subtraction step to simplify computation.

In the proposed *L-SwiGLU* model, the standard MLP is replaced with a Swish-Gated Linear Unit (SwiGLU)-based MLP to enhance performance [23]. Recognizing that not all information within each token contributes equally to predicting the location, we incorporated the Gated Linear Unit (GLU) within the MLP block to enable the model to focus on the most relevant features. Acting as an effective denoiser, the GLU is particularly beneficial in wireless communication scenarios where filtering out irrelevant data is critical. The GLU achieves this by performing a component-wise product of two linear projections of size $h_{\text{dim}}^{\text{SwiGLU}}$, selectively passing meaningful information.

$$\text{SwiGLU}_j(\tilde{\mathbf{Z}}_j^{\text{MHA}}) = \left(\text{Swish}(\tilde{\mathbf{Z}}_j^{\text{MHA}} \mathbf{W}_j^1) \odot (\tilde{\mathbf{Z}}_j^{\text{MHA}} \mathbf{W}_j^2) \right) \mathbf{W}_j^3. \quad (16)$$

The modified MLP block, referred to as SwiGLU, processes the input $\tilde{\mathbf{Z}}_j^{\text{MHA}}$ through a gating mechanism, as illustrated in Fig. 6. Specifically, the input undergoes two linear

projections, $\tilde{\mathbf{Z}}_j^{\text{MHA}} \mathbf{W}_j^1$ and $\tilde{\mathbf{Z}}_j^{\text{MHA}} \mathbf{W}_j^2$. One of these projections, $\tilde{\mathbf{Z}}_j^{\text{MHA}} \mathbf{W}_j^1$, is passed through the Swish activation function, which enables non-linear transformations essential for capturing complex patterns. The activated output is then combined with the second projection via a Hadamard product (\odot), creating a selective gating mechanism that prioritizes relevant features while suppressing noise. The resulting representation is projected through a final linear transformation \mathbf{W}_j^3 .

The output of the j^{th} encoder block is computed as:

$$\tilde{\mathbf{Z}}_j^{\text{ENC}} = \text{SwiGLU}_j \left(\text{RMSNorm} \left(\tilde{\mathbf{Z}}_j^{\text{MHA}} \right) \right) + \tilde{\mathbf{Z}}_j^{\text{MHA}}, \quad (17)$$

where the output of the MHA block, $\tilde{\mathbf{Z}}_j^{\text{MHA}}$, is first normalized using RMSNorm and then processed by the SwiGLU block (16). The resulting transformed representation is combined with the residual MHA output $\tilde{\mathbf{Z}}_j^{\text{MHA}}$ (11), thereby enhancing representational capacity while preserving gradient stability.

2) **Modifications Outside the Transformer Encoder Block:** In the vanilla ViT model, a class token \mathbf{X}_{cls} is appended to the input sequence to capture the global representation, which is subsequently used for prediction. However, the inclusion of the class token introduces an additional token to those generated during tokenization from PDP. Since the MHA layer exhibits quadratic complexity with respect to the number of tokens (\tilde{N}_{tk}), this addition significantly increases the computational complexity. To address this issue, the class token mechanism is replaced with a Global Average Pooling (GAP) layer. The GAP layer, placed after the N_L Transformer encoder, replaces the class token mechanism by aggregating information from all tokens through averaging across the token dimension. This approach enables the model to utilize the collective representation for prediction while significantly reducing computational overhead. In this case, the total number of tokens in the embedding $\mathbf{X}_{\text{emb}} = [\mathbf{X}_{\text{inp}}] \in \mathbb{R}^{\tilde{N}_{\text{tk}} \times D_{\text{emb}}}$ becomes $\tilde{N}_{\text{tk}} = N_{\text{tk}}$. The RMS normalization is applied on top of the aggregated information from the GAP layer, ensuring a well-normalized representation. This normalized output is then passed to the IH for the final prediction:

$$\hat{\mathbf{y}} = \text{IH} \left(\text{RMSNorm} \left(\text{GAP}(\tilde{\mathbf{Z}}_{N_L}^{\text{ENC}}) \right) \right). \quad (18)$$

Furthermore, due to the proposed tokenization approach described in Section V, positional embeddings are no longer required. In this approach, the entire sequence of sensor data is treated as a single token, and since the sensor positions are fixed, the positional order is inherently stored within the token itself. As a result, the positional embedding layer used in the vanilla Transformer can be omitted, simplifying the model architecture and reducing computational overhead:

$$\tilde{\mathbf{Z}} = \mathbf{X}_{\text{emb}}. \quad (19)$$

An additional advantage of eliminating positional embeddings is that it prevents the introduction of bias into token representations, which can disrupt the modeling of multivariate correlations. By removing positional embeddings, the proposed model retains the integrity of token information, enhancing the MHA block’s capability to accurately capture complex multivariate dependencies.

VI. EVALUATION AND ANALYSIS

For wireless sensor applications, computation and energy resources are typically highly constrained. In this study, to

evaluate the performance of the proposed model and tokenization approach, we consider small, medium, and large transformer models, each with strict limits on the number of FLOPs: 4.5M, 16.5M, and 63.5M FLOPs, respectively. These constraints enable a comprehensive analysis of how data requirements and computational demands vary across models of different sizes.

The remaining part of this section is structured as follows. First, we outline the training approach. Next, we provide a comparison of the proposed tokenization methods with the vanilla architecture. Finally, we evaluate the proposed *L-SwiGLU* architecture, utilizing the *SST* method, against the vanilla transformer.

A. Training Approach

The availability of large datasets has been a major contributor to the success of DL models. However, collecting large quantity of RF data and the corresponding ground truth device locations is very costly and time-consuming. There is hence a strong need for effective data augmentation techniques to alleviate the data collection burden. We adopt the three RF data augmentation techniques introduced in [13] and summarize them briefly in the following.

1) **Random Signal Dropping:** Out of the 18 received PDPs, we determine the number of PDPs to drop (set to all zeros) via

$$D = D_{\max}\beta, \quad (20)$$

where D_{\max} is the maximum number of PDPs that can be dropped, which is set to 7, and β is beta distributed with parameter set to (0.1,0.1). The beta distribution parameter is chosen such that no PDP is dropped roughly half the time and D_{\max} PDPs are dropped roughly half of the time. This emulates scenarios where some sensor nodes might be noisy, corrupted, or missing in real-world wireless applications.

2) **Random Signal Shifting:** Each of the 18 TD PDPs is independently shifted by a random amount along the time axis:

$$\left\{ \overset{\leftrightarrow}{p} [d] \right\}_d \triangleq \sum_{a=0}^{A-1} \left| \text{IFFT}_{N_{\text{FFT}}} \left(\left\{ e^{-j2\pi k \Delta_f \delta} H_a[k] \right\}_{k=-\frac{N}{2}}^{\frac{N}{2}-1} \right) \right|^2, \quad (21)$$

where δ follows a zero-mean truncated normal distribution with parameter σ_{RSS}^2 and limits of $(-2\sigma_{\text{RSS}}, 2\sigma_{\text{RSS}})$. This mimics the effect of network synchronization or transmit/receive timing offsets between the sensors and device, which are common impairments in real-world scenarios. We follow the suggested setting of $\sigma_{\text{RSS}} = 25$ ns.

3) **Smoothed Regression Mixup (SRM):** This is an improved mixup approach for regression problems. Two data samples, A and B, with the dimension 18×256 PDPs, x_A and x_B , are selected from a mini-batch to synthesize a new mixup PDP: $x_C = \lambda x_A + (1 - \lambda)x_B$, based on the probability given by a Gaussian kernel $\exp\left(-\frac{d(A,B)}{2\sigma_{\text{mix}}^2}\right)$ [24]. Here, λ is a beta distributed random mixing ratio with parameter (2,2), $d(A,B)$ is a similarity measure between the two data samples, and σ_{mix}^2 is a hyperparameter. The probability kernel is designed such that two samples more similar to each other are more likely used as mixup inputs, while two rather different samples are rarely paired for mixing. Given the mixup PDP input of x_C , the loss function for the model output \hat{y}_C is computed as the weighted average of the L_1 losses against the pre-mixing labels:

$$\text{loss}_{\text{SRM}} = \lambda \|\hat{y}_C - y_A\|_1 + (1 - \lambda) \|\hat{y}_C - y_B\|_1. \quad (22)$$

To reduce complexity, we compute the similarity measure by $d(A,B) \triangleq \|p_A - p_B\|_2^2$, where p_A and p_B are the device 2D coordinates, and set $\sigma_{\text{mix}}^2 = 4$. This results in SRM selecting $A = B$ with roughly 50% probability. That is, roughly half of the data samples in a mini-batch are replaced with synthetic ones while the other half are unmodified by SRM.

For training, we use the JAX framework from Google and a batch size of $B = 400$ PDPs sampled from the trainset with 40,000 PDPs. Network parameters are updated by the Adam algorithm with its default settings and a weight decay factor of 0.001. We use a cosine learning rate schedule with a warm-up that varies between $1e^{-5}$ and $2e^{-3}$ over 2000 training epochs. All test results are evaluated using a separate set of 4,000 test PDPs. Instead of selecting the model based on the best validation performance or using the weights from the last epoch, we use the Exponential Moving Average (EMA) of the model parameters with a decay rate of $\alpha = 0.9$. This smooths out fluctuations in the parameters, leading to more stable and reliable weights. At each step, the EMA is updated as:

$$\theta_t^{\text{EMA}} = \alpha \cdot \theta_{t-1}^{\text{EMA}} + (1 - \alpha) \cdot \theta_t, \quad (23)$$

where, θ_t^{EMA} and $\theta_{t-1}^{\text{EMA}}$ represent the EMA at epoch t and $t - 1$, respectively, while θ_t denotes the model weight at epoch t .

B. Performance Analysis of the Proposed Tokenization Methods

The FLOPs complexity and model specifications are greatly influenced by the tokenization approach used. Table I details the Transformer model specifications, with three values in each category being: $\{N_L, D_{\text{emb}}, h_{\text{dim}}\}$. For instance, $\{5,12,18\}$, vanilla Transformer architecture consists of 5 encoder blocks with embedding dimension $D_{\text{emb}} = 12$, and hidden dimension $h_{\text{dim}} = 18$. The number of attention heads is fixed at $N_h = 6$, and σ is defined as the Rectified Linear Unit (ReLU) for all approaches. For the PBT framework, W_h and W_w are defined as 8 and 3, respectively, resulting in a total of $N_{\text{tk}} = 96$ tokens. Each token is represented as a vector of length $N_{\text{st}} = 24$.

TABLE I: Transformer model configurations.

Model	<i>PBT</i>	<i>TST</i>	<i>SST</i>	FLOPs
Small	{5,12,18}	{3,12,18}	{6,48,68}	4.5 M
Medium	{8,24,44}	{5,24,44}	{10,72,122}	16.5 M
Large	{16,36,86}	{13,30,86}	{16,96,316}	63.5 M

The performances of the three tokenization methods are evaluated by analyzing the Cumulative Distribution Function (CDF) of the 2D positioning error for the device, as illustrated in Fig. 7. The figure presents the CDF results for a large *Vanilla Transformer* model evaluated across small, medium, and large datasets (from left to right) using all three tokenization methods. It is observed that the proposed *SST* tokenization method consistently outperforms the other two methods, namely *PBT* and *TST*, achieving a significant performance improvement in all three cases. In Fig. 7c *SST* method outperforms other tokenization methods, achieving a 90th percentile (Δ_{90}) error of 0.388 m. In comparison, *PBT* and *TST* report Δ_{90} errors of 0.659 m and 0.694 m, respectively. These findings indicate that *SST* effectively captures environmental dependencies and multivariate correlations, enhancing model performance, while the other

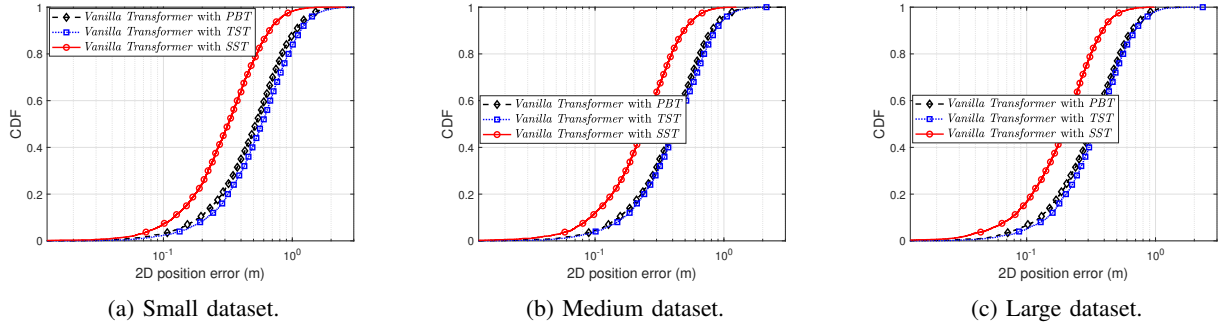


Fig. 7: Comparison of the CDF of 2D positioning errors for large models on different dataset sizes, evaluated across three tokenization methods using the *Vanilla Transformer*.

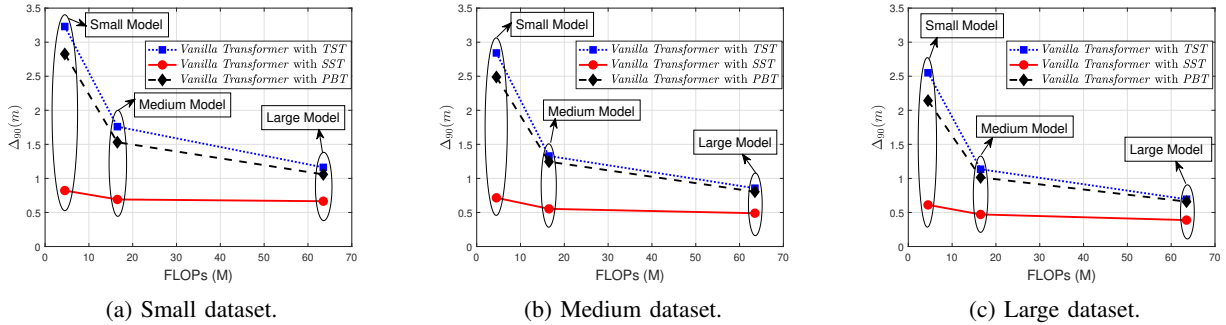


Fig. 8: Comparison of Δ_{90} positioning errors for varying model and dataset sizes, evaluated across three tokenization methods using the *Vanilla Transformer*.

methods fuse information from distinct sensors which leads to poor performance.

It can be observed that as the dataset size increases (from Fig. 7a to Fig. 7c), the CDF curve shifts to the right, indicating a reduction in positioning error. Specifically, for the Δ_{90} error, the *TST* tokenization method demonstrates a percentage improvement of 26.34% when the dataset increases from small to medium, and 40.28% when increasing from small to large. Similarly, for the *PBT* tokenization method, the percentage improvement is 24.08% for a small to medium dataset increase, and 37.77% for a small to large dataset increase. In comparison, the proposed *SST* tokenization method exhibits a percentage improvement of 26.47% as the dataset grows from small to medium, and 40.75% when transitioning from small to large. These results highlight that while all tokenization methods benefit from larger datasets, the proposed *SST* achieves superior improvements. Furthermore, the comparatively lower percentage improvements of *TST* and *PBT* suggest that their suboptimal tokenization strategies limit the model’s ability to effectively leverage larger datasets, whereas *SST* demonstrates its capability to harness the additional data for enhanced performance.

Fig. 8 illustrates the Δ_{90} errors for small, medium, and large models across datasets of varying sizes. As shown in Fig. 8a, the Δ_{90} error for all model sizes trained on the small dataset indicates that the proposed *SST* consistently achieves the lowest positioning errors. A similar trend is observed in Fig. 8b and 8c, where the Transformer models are trained on medium and large datasets. Comparing the Δ_{90} error of the small, medium, and large models trained on the large dataset, the proposed tokenization method achieves percentage improvements of 76.06%, 58.53%, and 44.08%, respectively, over the *TST*. Despite having the same computational complexity in terms of FLOPs, the performance gap between the models is notable, emphasizing the

effectiveness of the proposed tokenization method.

Considering model complexity, the model trained on a small dataset using *SST* (see Fig. 8a) achieves superior positioning accuracy. Notably, the small model trained with the proposed *SST* tokenization method not only outperforms models of similar size but also surpasses both medium and large models trained with *PBT* and *TST* tokenization techniques. Specifically, the small model using *SST* achieves a 70.92% improvement over models with comparable computational complexity. Furthermore, it demonstrates a 46.31% improvement compared to a model 3.66 times larger trained with *PBT* and achieves a 22.38% improvement over a model 14.1 times larger trained with *PBT*. These results highlight that efficient tokenization can achieve higher accuracy with lower computational requirements, as also observed in Fig. 8b and 8c.

The Δ_{90} error for the large model trained on the small dataset using the proposed *SST* tokenization method is 0.665 m. In comparison, the Δ_{90} error for the large model trained on the large dataset is 0.694 m with *TST* and 0.659 m with *PBT*. Notably, the model trained on the small dataset using *SST* outperforms the large dataset model using *TST*, while achieving results comparable to those of the large dataset model using *PBT*. These results demonstrate that the proposed *SST* method significantly reduces the model’s reliance on dataset size.

In all three subfigures, it is evident that as the model size increases, the Δ_{90} error decreases. This trend is attributed to the larger models’ enhanced capacity to capture the intricate variations and complex relationships within the dataset. Specifically, the Δ_{90} error of the proposed *SST* approach for the small model trained on the small dataset is 0.882 m, whereas the error for the small model trained on the large dataset reduces to 0.665 m. In contrast, when the large model is trained on the large dataset, the Δ_{90} error decreases to 0.388 m. This suggests that the small

model does not fully benefit from the larger dataset, likely due to the increased variability in the data, while the large model is better equipped to capture the complex behavior of the data more efficiently. Notably, for all model sizes, the proposed tokenization approach consistently outperforms others, demonstrating its effectiveness in reducing reliance on large datasets by efficiently capturing channel independence and multivariate correlations.

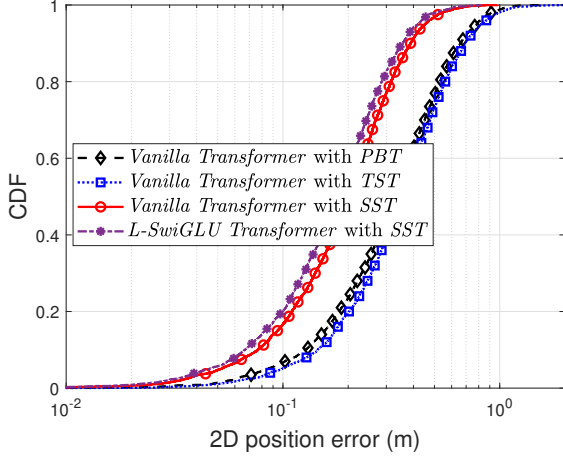


Fig. 10: The CDF of 2D positioning errors for large *L-SwiGLU* model trained on large dataset using *SST* is shown alongside the CDFs of all tokenization methods already presented in Fig. 7c.

C. Performance Analysis of the Proposed *L-SwiGLU ViT*

The proposed *L-SwiGLU* model architecture shares a similar parameter configuration with the *Vanilla Transformer* for *SST* (Table. I), differing primarily in the hidden dimension, denoted as $h_{\text{dim}}^{\text{SwiGLU}}$. For the small, medium, and large models, the values of $h_{\text{dim}}^{\text{SwiGLU}}$ are 54, 94, and 231, respectively. These values are chosen such that the model complexity, in terms of FLOPs, remains equivalent to that of the *Vanilla Transformer*, ensuring a fair comparison. The number of encoder blocks (N_L), embedding dimension (D_{emb}), and attention heads ($H = 6$) remain identical to those of the *Vanilla Transformer*, as summarized in Table I.

As the proposed *SST* tokenization method has consistently demonstrated superior performance across all cases, this subsection focuses exclusively on evaluating the proposed *L-SwiGLU Transformer* using the *SST* tokenization.

Fig. 10 presents the CDF of 2D positioning errors for the proposed *L-SwiGLU Transformer* with *SST* tokenization

and compares it against the *Vanilla Transformer* utilizing all three tokenization methods: *PBT*, *TST*, and *SST*. The results correspond to the scenario where a large model is trained on a large dataset. Despite maintaining similar computational complexity, the proposed *L-SwiGLU Transformer* achieves notably better performance, outperforming the *Vanilla Transformer*. Specifically, the Δ_{90} positioning error (Δ_{90}) for the *Vanilla Transformer* is 0.388 m, whereas the proposed *L-SwiGLU Transformer* achieves a reduced error of 0.355 m, demonstrating its superior accuracy and efficiency in large-scale scenarios.

The Fig. 9 demonstrates the percentage improvement in 2D positioning errors achieved by the *L-SwiGLU Transformer* over the *Vanilla Transformer* with proposed *SST* method across small, medium, and large models for three dataset sizes (small, medium, and large) at the 50th, 67th, 80th, and 90th percentiles. It can be seen that the proposed *L-SwiGLU Transformer* model demonstrates a positive percentage improvement, indicating its superior performance over the *Vanilla Transformer*. Across all model configurations (Fig. 9a to Fig. 9c), the large dataset consistently delivers the most significant performance gains, as it provides richer and more diverse training samples, enabling the model to better learn complex patterns and generalize effectively.

For the large dataset, the small model demonstrates a percentage improvement ranging from 10.15% to 11.18%, while the medium model shows a decrease to 8.91% to 7.22%. For the large model, the improvement ranges from 10.08% to 8.51%. The higher percentage improvement observed in the small model is attributed to its previously limited ability to fully utilize the large dataset when trained with the *Vanilla Transformer*. With the proposed *L-SwiGLU Transformer* model, the small model is now able to effectively leverage the large dataset, resulting in significant performance gains.

For the small and medium models (Fig. 9a, and Fig. 9b), improvements are moderate for the medium dataset and highest for the large dataset, while the small dataset yields limited gains. For the large model, the performance improvement on the small dataset is minimal at the 50th and 67th percentiles. However, at the (Δ_{90}), the proposed *L-SwiGLU Transformer* demonstrates superior performance. As the model size increases, the percentage improvement becomes more sensitive to dataset size, reinforcing the need for appropriately scaled datasets to realize the full potential of larger models.

Fig. 11 presents the Δ_{90} positioning error for the proposed *L-SwiGLU Transformer* using *SST* compared to the *Vanilla Transformer* across different tokenization methods

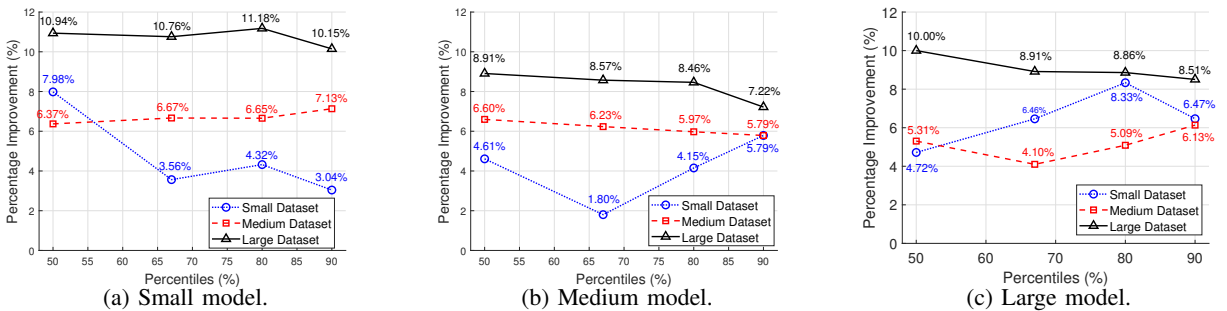


Fig. 9: Percentage improvement in 2D positioning errors of the proposed *L-SwiGLU Transformer* over the *Vanilla Transformer* using proposed *SST* tokenization for small, medium, and large models across three datasets at the 50th, 67th, 80th, and 90th percentiles.

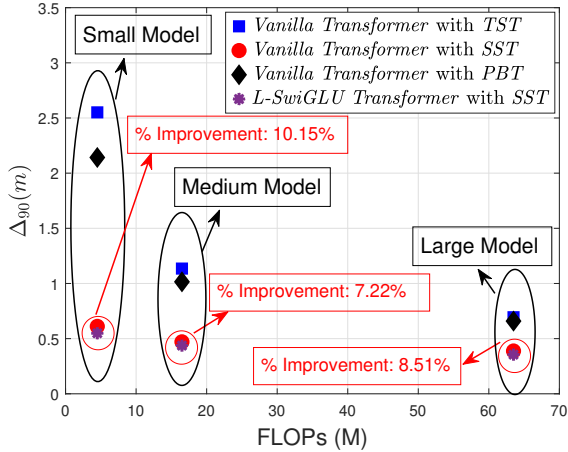


Fig. 11: Comparison of Δ_{90} positioning errors for the *L-SwiGLU Transformer* across varying model sizes on the large dataset, with the *Vanilla Transformer* using three tokenization methods.

on the large dataset. The *L-SwiGLU Transformer* with *SST* consistently achieves superior performance. Despite having similar computational complexity, the percentage improvement of the *L-SwiGLU Transformer* over the *Vanilla Transformer* (both using *SST*) ranges from 7.22% to 10.15%. Compared to the *Vanilla Transformer* using *TST*, the percentage improvements are 78.48%, 61.50%, and 48.85% for the small, medium, and large datasets, respectively. Similarly, improvements over the *Vanilla Transformer* with *PBT* are 74.37%, 56.95%, and 46.13%. The proposed *L-SwiGLU Transformer* demonstrates superior performance compared to the *Vanilla Transformer* models with *PBT* of significantly larger sizes. Specifically, the small *L-SwiGLU Transformer* outperforms the medium *Vanilla Transformer* trained with *PBT*, which is 3.75 times larger, achieving a 66.99% improvement. It also surpasses the large *Vanilla Transformer* with *PBT*, which is 14.1 times larger, with a 46.13% improvement. When compared to the *Vanilla Transformer* with *SST*, the improvements over *PBT* are 46.31% and 22.38%, respectively, as detailed in Subsection VI-B. These results highlight the substantial performance improvements achieved by the proposed *SwiGLU*, with percent gains significantly increasing from 46.31% to 66.99% and from 22.38% to 46.13%. These results highlight the effectiveness of the proposed *SST* tokenization and the significant performance gains achieved by the *L-SwiGLU Transformer*.

VII. CONCLUSION

In this paper, we investigated the application of the Transformer model for indoor localization in highly NLOS environments. Specifically, we focused on the often overlooked aspect of the Transformer architecture—tokenization—and its potential impact on wireless communication applications. We proposed an efficient *SST* method that transforms the information received by each sensor into diverse tokens, effectively capturing the channel dependencies between sensors. The proposed tokenization method addresses the challenge of improving localization accuracy while reducing computational overhead and dependence on large datasets. Through this innovation, the Transformer model achieved state-of-the-art performance, demonstrating a Δ_{90} error of just 0.388 m in a high NLOS indoor factory scenario, while

outperforming a model 14.1 times larger that employs conventional tokenization, achieving a percentage improvement of 22.38%.

Furthermore, an efficient Transformer model, *L-SwiGLU*, is proposed, leveraging the GLU activation to enhance de-noising capabilities by filtering out irrelevant data in wireless communication scenarios. GLU, combined with removing bias induced by positional embeddings and other modifications, allows the *L-SwiGLU* model to focus on essential features, improving robustness. The proposed model, when combined with the *SST* tokenization method, achieves an 8.51% improvement in performance over the *Vanilla Transformer*. The evaluation across various model and dataset sizes demonstrates a reduced dependence of Transformer models on large datasets when utilizing the proposed method. Moreover, smaller models fail to leverage larger datasets due to their limited learning and representational capacity. This result highlights the effectiveness of using the modified Transformer to model the complex intricacies of RF propagation. This work contributes to the efficient adoption of Transformer models in wireless communication, particularly in the domain of RF positioning. Future work will focus on reducing Transformer architecture complexity and scaling the model for improved efficiency and performance.

REFERENCES

- [1] H. Lee, B. Lee, H. Yang, J. Kim, S. Kim, W. Shin, B. Shim, and H. V. Poor, "Towards 6G hyper-connectivity: Vision, challenges, and key enabling technologies," *J. Commun. Net.*, vol. 25, no. 3, pp. 344–354, Jun. 2023.
- [2] L. T. Nguyen, J. Kim, S. Kim, and B. Shim, "Localization of IoT networks via low-rank matrix completion," *IEEE Trans. Commun.*, vol. 67, no. 8, pp. 5833–5847, Aug. 2019.
- [3] N. Singh, S. Choe, and R. Punmiya, "Machine learning-based indoor localization using Wi-Fi RSSI fingerprints: An overview," *IEEE Access*, vol. 9, pp. 127 150–127 174, Sep. 2021.
- [4] S. Shang and L. Wang, "Overview of Wi-Fi fingerprinting-based indoor positioning," *IET Commun.*, vol. 16, no. 7, pp. 725–733, Apr. 2022.
- [5] A. Vaswani, N. Shazeer, N. Parmar, J. Uszkoreit, L. Jones, A. N. Gomez, L. Kaiser, and I. Polosukhin, "Attention is all you need," in *Proc. Advances in Neural Inf. Process. Syst. (NeurIPS)*, vol. 30, Long Beach, CA, Dec. 2017, pp. 5998–6008.
- [6] S. Khan, M. Naseer, M. Hayat, S. W. Zamir, F. S. Khan, and M. Shah, "Transformers in vision: A survey," *ACM computing surveys (CSUR)*, vol. 54, no. 10s, pp. 1–41, 2022.
- [7] A. Dosovitskiy, L. Beyer, A. Kolesnikov, D. Weissenborn, X. Zhai, T. Unterthiner, M. Dehghani, M. Minderer, G. Heigold, S. Gelly, J. Uszkoreit, and N. Houlsby, "An image is worth 16x16 words: Transformers for image recognition at scale," in *Proc. Int. Conf. Learn. Represent. (ICLR)*, Vienna, Austria (Virtual Conf.), May 2021.
- [8] F. Alhomayani and M. H. Mahoor, "Deep learning methods for fingerprint-based indoor positioning: A review," *J. Locat. Based Serv.*, vol. 14, no. 3, pp. 129–200, Sep. 2020.
- [9] M. Nasir, K. Esguerra, I. Faye, T. B. Tang, M. Yahya, A. Tummian, and E. T. W. Ho, "HyTra: Hyperclass Transformer for Wi-Fi fingerprinting-based indoor localization," *Trans. Energy Syst. Eng. Appl.*, vol. 5, no. 1, pp. 1–24, Jan. 2024.
- [10] M. T. Hoang, B. Yuen, K. Ren, X. Dong, T. Lu, R. Westendorp, and K. Reddy, "A CNN-LSTM quantifier for single access point CSI indoor localization," *arXiv preprint arXiv:2005.06394*, 2020.
- [11] K. Gao, H. Wang, H. Lv, and W. Liu, "Toward 5G NR high-precision indoor positioning via channel frequency response: A new paradigm and dataset generation method," *IEEE J. Sel. Areas Commun.*, vol. 40, no. 7, pp. 2233–2247, Jul. 2022.
- [12] J. F. Cheng, A. R. Khamesi, and Y. Blankenship, "Complex-valued neural networks for distributed machine learning assisted RF positioning," in *Proc. IEEE Mil. Commun. Conf. (MILCOM)*, Washington, DC, Oct. 2024.
- [13] J.-F. Cheng, A. Khamesi, and E. Gudmundson, "Complex-valued convolutional networks for precise positioning in NLoS environment with distributed mimo," *Under Review*, 2025.
- [14] W. Li, X. Meng, Z. Zhao, Z. Liu, C. Chen, and H. Wang, "LoT: A Transformer-based approach based on channel state information for indoor localization," *IEEE Sens. J.*, vol. 23, no. 16, pp. 18 654–18 666, Aug. 2023.
- [15] H. Zhou, J. Yang, S. Deng, and W. Zhang, "VTIL: A multi-layer indoor location algorithm for RSSI images based on vision Transformer," *Eng. Res. Express*, vol. 6, no. 1, p. 015069, Jan. 2024.
- [16] A. S. Lutakamale, H. C. Myburgh, and A. De Freitas, "A hybrid convolutional neural network-transformer method for received signal strength indicator fingerprinting localization in long range wide area network," *Eng. Appl. Artif. Intell.*, vol. 133, p. 108349, Jan. 2024.

- [17] G. Prasad, A. Gupta, A. Aryan, and S. Kumar, "A vision transformer-based indoor localization using CSI signals in IoT networks," in *Proc. Int. Conf. Adv. Inf. Netw. Appl. (AINA)*, Tokyo, Japan, Mar. 2024, pp. 73–83.
- [18] X. Xu, F. Zhu, S. Han, Z. Yu, H. Zhao, B. Wang, and P. Zhang, "Swin-Loc: Transformer-based CSI fingerprinting indoor localization with MIMO ISAC system," *IEEE Trans. Veh. Technol.*, vol. 73, no. 1, pp. 123–135, Jan. 2024.
- [19] J. Pan, K. Yin, and B. Wu, "A Transformer-based method for the single-target location in wireless sensor networks," in *Proc. IEEE Int. Conf. Appl. Mach. Learn. (ICAML)*, Chengdu, China, Dec. 2022, pp. 260–265.
- [20] F. Luo, S. Khan, B. Jiang, and K. Wu, "Vision transformers for human activity recognition using Wi-Fi channel state information," *IEEE Internet Things J.*, vol. 11, no. 1, pp. 123–135, Jan. 2024.
- [21] 3GPP Technical Report 38.901: Study on channel model for frequencies from 0.5 to 100 GHz, Tech. Rep., 2019. [Online]. Available: <https://www.3gpp.org/specifications>.
- [22] B. Zhang and R. Sennrich, "Root mean square layer normalization," in *Proc. Advances in Neural Information Processing Systems (NeurIPS)*, vol. 32, Vancouver, Canada, Dec. 2019.
- [23] N. Shazeer, "GLU variants improve Transformer," *arXiv preprint arXiv:2002.05202*, 2020.
- [24] H. Yao, Y. Wang, L. Zhang, J. Y. Zou, and C. Finn, "C-Mixup: Improving generalization in regression," in *Proc. Advances Neural Inf. Process. Syst. (NeurIPS)*, vol. 35, New Orleans, LA, Dec. 2022, pp. 3361–3376.